International Journal of Innovative Technology and Exploring Engineering (IJITEE)
ISSN: 2278-3075 (Online), Volume-9 Issue-6, April 2020

Corrosion and Inhibitor on Material: Experimental and Computational Calculations

Aezeden Mohamed, Ahmad Alrawashdeh, Abdalhamid Rahoma

Abstract*: *In this paper, we provide a comprehensive study of corrosion inhibition of mild steel in 1 M HCl solution at 313, 323, and 333 K using 4,4-Dimethyl oxazolidine-2-thione (DMOT) and its protonated form ($DMOTH^+$) as inhibitors. Our results show that the corrosion rate of mild steel in 1 M HCl increases as the temperature increases while it decreases as the DMOT concentration increases. In contrast to the corrosion rate, the DMOT inhibition efficiency decreases with temperature and increases with increasing DMOT concentration. Both experimental and quantum chemical computational results reveal that the adsorption of DMOT and $DMOTH^+$ on the mild steel surface is a mixed-type process having both physisorption and chemisorption. Moreover, the inhibitor adsorption on the mild steel surface was found to obey the Langmuir adsorption isotherm and the value of Gibbs energy of adsorption at the three studied temperatures is associated with an adsorption mechanism involving both physisorption and chemisorption processes. Heavy corrosion, cavities, and pitting of surfaces were observed in the absence of DMOT inhibitor, while much less corrosion was consistently observed in the presence of DMOT inhibitor.

Keywords:* *Keywords: corrosion, corrosion inhibition, density functional theory, inhibition efficiency, mild steel.

I. INTRODUCTION

Besides being one of the least expensive steel, mild steel also combines many attractive properties including weldability, durability, hardenability, and suitability for heat treatment [1-5]. These properties allow for a wide range of applications of mild steel in construction, frame structures, machinery tools, pipelines, and many others [6-8]. However, the most severe and commonly experienced drawback of mild steel is its susceptibility to corrosion especially in acidic environments [9]. It is susceptible to several forms of corrosive attacks such as stress corrosion, galvanic corrosion, uniform corrosion, pitting corrosion, and crevice corrosion [10]. Because of the enormous economic losses and safety hazards associated with mild steel corrosion every year worldwide, prevention and control are essential and unavoidable [5,11,12].

Revised Manuscript Received on April 30, 2020.
***** Correspondence Author
Aezeden Mohamed*, Faculty of Engineering and Applied Sciences, Mechanical Engineering Department, PNG University of Technology, Lae, MP 411, Papua New Guinea. *E-mail: aezeden.mohamed@pnguot.ac.pg
Ahmad Alrawashdeh, Department of Physics and Physical Oceanography, Memorial University of Newfoundland, St. John's, NL, A1B 3X7, Canada. amohamed@mun.ca
Abdalhamid Rahoma, Faculty of Engineering and Applied Sciences

Although several methods have been developed for controlling and preventing mild steel corrosion, this study focuses on the use of corrosion inhibitors.

A corrosion inhibitor is an organic or inorganic chemical substance added to a corrosive medium in order to control corrosion rates. Organic inhibitors contain one or more electron-rich atoms (i.e., O, N, S, or P), unsaturated, or π-conjugated bonds that can interact with metal atoms or adsorbed on the metal surface [23-30]. Inhibitors reduce corrosion rates by one of the following mechanisms: formation of a thin-film through chemical adsorption (chemisorption) of the inhibitor on the metal surface, the inhibitor enhancing the formation of a thin layer of metal oxide, or the formation of a complex compound by a chemical reaction between the inhibitor and corrosive components in the solution [16].

Immense research efforts have been devoted over many years to the study of corrosion prevention and control of iron and its alloys by inhibitors [1,12-22,29-31]. Resit Yildiz used 4,6-diamino-2- pyrimidinethiol as an inhibitor to investigate corrosion inhibition of mild steel in HCl solutions using experimental and computational techniques [12]. Bouanis et al. showed that 2,5-bis(4-dimethylaminophenyl)-1,3,4-oxadiazole acts as an efficient inhibitor of carbon steel corrosion in 1 M HCl solution [21]. Recently, a novel green inhibitor extract of Melia Azedarach (MA) seeds was used for preventing corrosion of carbon steel in 2.0 mol L^{-1} HCl solution by El-Etre and Ali [22]. Their results show that MA extract inhibits both cathodic and anodic steel reactions, and its efficiency increases by increasing its concentration. Musa and his co-authors [1] conducted a comparative study of the corrosion inhibition of mild steel in 2.5 M H_2SO_4 solution by 4,4-dimethyloxazolidine-2-thione (DMOT) at different temperatures. They found that DMOT exhibits excellent inhibition performance as a mixed-type inhibitor and its efficiency increases as its concentration increases, but it decreases as the temperature increases. In another study [31], Musa et al. utilized DMOT to study the corrosion inhibition of mild steel in 1 M HCl at 30°C using electrochemical and quantum chemical calculations. Their results showed that adsorption of DMOT on the mild steel surface is a chemisorption type in which DMOT donates electron to mild steel atoms, and that the area around the S atom in DMOT is the most probable site for bonding with the mild steel surface.

In this study, we investigate the effect of temperature and concentration on inhibition performance and efficiency of 4,4-dimethyloxazolidine-2-thione (DMOT) inhibitor and its protonated form on mild steel in 1 M HCl solution using a variety of experimental and quantum chemical calculation techniques (chemical structure of DMOT is shown in Figure

1). The main objectives of this work are: (i) to provide new insights into the corrosion inhibition mechanism of DMOT on mild steel in HCl solutions, and (ii) to investigate the effect of temperature and inhibitor concentration on the inhibition performance and efficiency of DMOT on mild steel in HCl solutions.

In order to achieve these goals, the dependence of mild steel corrosion on different temperatures (i.e., 313, 323, and 333 K) and inhibitor concentrations (i.e., 0.1, 0.4, 1.0, 2.0, 4.0 mM) was examined. Potentiodynamic Polarization was conducted to calculate polarization parameters and corrosion rates. Thermodynamic and kinetic parameters, scanning electron microscopy (SEM), energy dispersive spectroscopy, and X-ray diffraction (XRD) analysis were obtained. In addition, quantum chemical computations were performed using density functional theory (DFT) to correlate the molecular structure and properties of DMOT and $DMOTH^+$ with their inhibition action.

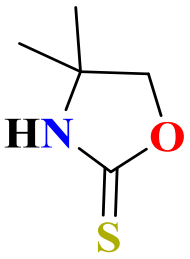

Fig. 1. The chemical structure of 4,4-dimethyloxazolidine-2-thione (DMOT) inhibitor.

II. EXPERIMENTAL PROCEDURES

A. Material

Mild steel specimens with an exposed area of 4.52 cm2 and a chemical composition (in wt. %) shown in Table 1 were used in this study.

Table 1: Chemical composition of mild steel specimens and values used for calculating corrosion rates.

Mild steel	Chem. Comp.	At. wt.	Density	Oxidation State	Fraction			
Comp.	wt%				Chem. Comp.	At. wt.	Density	Oxidation State
Fe	99.21	55.85	7.87	2	0.9797	54.7129	7.7144	1.9595
C	0.21	12.01	2.27	4	0.0096	0.1158	0.0219	0.0386
Si	0.38	28.09	2.33	4	0.0075	0.2096	0.0174	0.0298
P	0.09	30.97	1.82	5	0.0016	0.0496	0.0029	0.0080
S	0.05	32.06	2.07	2	0.0009	0.0276	0.0018	0.0017
Mn	0.05	54.94	7.44	2	0.0005	0.0276	0.0037	0.0010
Al	0.01	26.98	2.70	3	0.0002	0.0055	0.0006	0.0006
Total	**100.00**	**240.89**	**26.50**	**22**	**1.0000**	**55.1485**	**7.7626**	**2.0392**

Prior to all experiments, the surfaces of specimens were abraded with a series of silicon carbides papers (grits from 400 to 1200). The specimens were then ultrasonically degreased in a detergent solution, rinsed with deionized water and dried with warm air, and then placed in an electrochemical cell according to ASTM Standard G1-03 [32]. All chemicals used were of reagent grade quality and solutions were prepared with deionized water. The chemical solutions used in this work (i.e., 0.1, 0.4, 1.0, 2.0, and 4.0 mM of DMOT and 1 M HCl) were freshly prepared before use.

B. Corrosion Measurements

Electrochemical experiments were carried out in a glass vessel containing 150 ml of the test solution and enclosed by a Gamry water-jacketed glass cell. The corrosion cell contains three electrodes: the working electrode (mild steel), the counter electrode (graphite), and the reference electrode (saturated calomel (SCE)). Potentiodynamic Polarization measurements were obtained by scanning the electrode potential from -0.75 to -0.25 V at a rate of 1 mV s-1 at 313, 323, and 333 K. Electrochemical measurements were initiated about 30 min after the immersion of the working electrode in solution in order to stabilize the steady state potential.

C. Scanning Electron Microscopy and Energy Dispersive Spectroscopy

Scanning electron microscopy (SEM) analyses were performed using a JEOL7100F field emission SEM equipped with a thermo energy dispersive spectroscopic (EDS) detector. Images were obtained after the immersion of mild steel specimens in 1 M HCl solution, first in the absence and then in the presence of 4mM DMOT for 3 h at 313, 323, and 333 K by the secondary electron image mode. The images were taken under a constant working voltage of 15 kV and under same scan and dead time at working distances of 11 and 12 mm with magnifications of x1000 at 313, 323 K and x100 at 333 K.

D. X-Ray Diffraction

The X-ray diffraction (XRD) patterns of the surfaces of mild steel specimens after immersing them in 1M HCl with and without 4 mM DMOT for 3 h at 313, 323, and 333 K were measured using a Rigaku Ultima-IV powder x-ray diffractometer equipped with a Cu source and a scintillation detector. The software used for identifying samples was MDI JADE 2010 with databases from ICDD and ICSD.

E. Quantum Chemical Computation Details

All computations in this study were performed using the Gaussian 09 program [33]. For all calculations, we employed the B3LYP [34,35] density functional method with the polarized split-valence double-ζ 6-31G(d) basis set. The geometries of DMOT and $DMOTH^+$ were fully optimized with B3LYP/6-31G(d) in the gas phase and in aqueous solution using the polarizable continuum model (PCM) [36]. The PCM was used to evaluate the effect of solvent (water) on the geometry, energetics, and charges distribution of DMOT and $DMOTH^+$. Energies of the highest occupied (E_{HOMO}) and the lowest unoccupied molecular orbitals (E_{LUMO}) and their gap (ΔE_{HL}) of both DMOT and $DMOTH^+$ were obtained in PCM. The ionization potential (I) and the electron affinity (A) are related to E_{HOMO} and E_{LUMO} by the following relations:

$$I = -E_{HOMO} \quad (1)$$

$$A = -E_{LUMO} \quad (2)$$

The absolute electronegativity (χ) and absolute hardness (η) are related to the ionization potential and electron affinity by

$$\chi = \frac{I + A}{2} \quad (3)$$

$$\eta = \frac{I - A}{2} \quad (4)$$

The softness (σ) is the inverse of the hardness.

$$\sigma = \frac{1}{\eta} \quad (5)$$

The number of electrons (ΔN) transferred between the frontier orbitals of the inhibitor and iron atoms was calculated using the following equation:

$$\Delta N = \frac{\chi_{Fe} - \chi}{2(\eta_{Fe} - \eta)} \quad (6)$$

where χ_{Fe} and χ are the absolute electronegativity of the iron and inhibitor, respectively, and η_{Fe} and η are the absolute hardness of the iron and inhibitor, respectively. We used values of $\chi_{Fe} = 7.0$ eV and $\eta_{Fe} = 0$ eV (assuming $I \approx A$ for metallic bulks) for Fe [37]. In order to determine which atom(s) in the inhibitor has the ability to accept or donate electrons, we have calculated Fukui functions through the finite difference approximation using Hirshfeld population analysis. The Fukui functions in the finite difference approximation are defined as follows,

$$f_k^+ = q_k(N+1) - q_k(N) \quad (7)$$

$$f_k^- = q_k(N) - q_k(N-1) \quad (8)$$

where N is the number of electrons in the molecule; and $q_k(N)$, $q_k(N+1)$, and $q_k(N-1)$ are the gross charge of atom k in the neutral molecule, anion, and cation respectively.

III. RESULTS AND DISCUSSION

A. Potentiodynamic Polarization Curves

Potentiodynamic polarization curves for mild steel specimens in 1 M HCl solution with the absence and presence of different concentrations (0.1, 0.4, 1.0, 2.0, and 4.0 mM) of DMOT at 313, 323, and 333 K are shown in Figure 2. From the anodic and cathodic curves of Figure 2, the corrosion potential (E_{corr}), the corrosion current density (I_{corr}), and the anodic and cathodic Tafel slopes (β_a and β_c) are obtained by the Tafel extrapolation method for all specimens at 313, 323, and 333 K. These polarization parameters are listed in Table 2 together with the degree of surface coverage (θ) and the inhibition efficiency ($IE\%$) that are determined using the formulae [4,28]:

$$\theta = \frac{I_{corr(blank)} - I_{corr(inh)}}{I_{corr(blank)}} \quad (9)$$

$$IE\% = \theta \times 100 \quad (10)$$

where $I_{corr(blank)}$ and $I_{corr(inh)}$ are the corrosion current densities in the absence and presence of inhibitor, respectively.

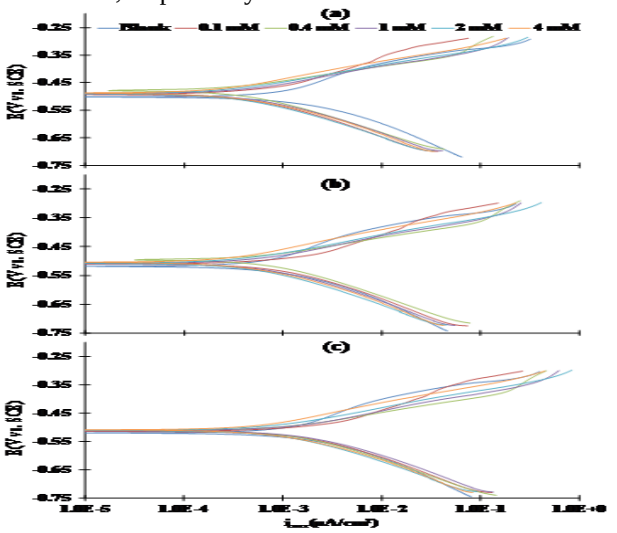

Fig. 2. Potentiodynamic polarization curves of mild steel corrosion in 1 M HCl solution with different DMOT concentrations at temperatures of; (a) 313 K, (b) 323 K, (c) 333 K.

Table 2: Polarization parameters of mild steel corrosion in 1 M HCl solution with different DMOT concentrations (mM) and temperatures (K). *

T	DMOT conc.	E_{corr}	i_{corr}	β_a	β_c	θ	IE%
313	Blank	0.498	1.260	0.071	0.159	0.000	00.0
	0.10	0.490	0.846	0.122	0.119	0.329	32.9
	0.40	0.478	0.412	0.159	0.085	0.673	67.3
	1.00	0.489	0.361	0.096	0.113	0.713	71.3
	2.00	0.488	0.243	0.094	0.118	0.807	80.7
	4.00	0.486	0.168	0.089	0.129	0.867	86.7
323	Blank	0.512	1.500	0.148	0.090	0.000	00.0
	0.10	0.505	1.040	0.071	0.060	0.307	30.7
	0.40	0.495	0.753	0.048	0.040	0.498	49.8
	1.00	0.504	0.514	0.163	0.181	0.657	65.7
	2.00	0.502	0.445	0.074	0.078	0.703	70.3
	4.00	0.502	0.324	0.129	0.107	0.784	78.4
333	Blank	0.515	2.650	0.077	0.056	0.000	00.0
	0.10	0.508	1.873	0.170	0.081	0.293	29.3
	0.40	0.508	1.390	0.063	0.046	0.475	47.5
	1.00	0.506	1.270	0.019	0.026	0.521	52.1
	2.00	0.504	0.911	0.266	0.271	0.656	65.6
	4.00	0.502	0.641	0.096	0.132	0.758	75.8

* β_a and β_c in (v dec^{-1}), i_{corr} in (mA cm^{-2}), E_{corr} in (V vs. SCE).

It can be seen from Table 2 and graphs (a), (b), and (c) in Figure 2 that, with the presence of DMOT, both anodic and cathodic Tafel curves shift toward lower I_{corr} values and slightly shift (< 13 mV) toward less positive E_{corr} values. Also, the values of both β_a and β_c change in the presence of DMOT inhibitor and when increasing its concentration. These observations suggest that DMOT is a mixed-type inhibitor [8,9] that reduces both the oxidation of Fe atoms (mild steel dissolution) and the reduction of H^+ ions (H_2 evolution reaction), and this inhibition effect increases as the concentration of DMOT raises. Slopes of the anodic and cathodic Tafel curves (that belong to different DMOT concentrations) in each of the graphs (a), (b), and (c) in Figure 2 are almost parallel, suggesting that the corrosion's mechanism is not influenced by the presence of the DMOT inhibitor and the DMOT simply acts as a barrier film preventing the acid from attacking the steel surface [12,13]. As the temperature increases, I_{corr} increases which implies the adsorption mechanism in which DMOT molecules are adsorbed on the mild steel surface. The surface coverage (θ) and inhibition efficiency (IE %) increase with increasing concentration of DMOT, while they decrease as the temperature increases.

Both observations are further evidence that DMOT is absorbed on the mild steel surface and, thereby, inhibits corrosion [15]. A maximum efficiency of inhibition by the DMOT of 86.7 % is achieved at a DMOT concentration of 4 mM at 313 K.

B. Corrosion Rate

In this work, corrosion rates (C_R), in cm/year, are calculated from the corrosion current density (I_{corr}) values (obtained from potentiodynamic polarization measurements) and the chemical composition of the mild steel specimens using the following equation [10]:

$$C_R = \frac{327\, I_{corr}\, A_W}{\rho N} \quad (4)$$

where A_W, ρ, and N are the average of atomic weights, densities, and oxidation states of the elements in the mild steel specimens, respectively. The constant (327) in the numerator of Eq. 4 includes the Faraday constant and time conversion factors. Table 1 presents all the information required to determine the corrosion rates including the chemical composition in (wt.%), and average of atomic weights, densities, and oxidation states of the mild steel specimens.

The calculated values of the mild steel corrosion rates as functions of temperature and DMOT concentration are summarized in Table 3 and depicted graphically in Figure 3. One can see from Table 3 and Figure 3 that the corrosion rate decreases as DMOT concentration increases and increases when the temperature increases. At a given temperature, there exists an equilibrium between adsorbed and desorbed DMOT molecules on the mild steel surface. Thus, the effect of temperature on the corrosion rate in the presence of DMOT can be understood as the increasing of temperature shifts the equilibrium state in the direction of the desorption process, which in turn increases the area of mild steel surface exposed to HCl and, therefore, increases the corrosion rate [14].

Table 3: Corrosion rate (cm/year) of mild steel in 1 M HCl with different DMOT concentrations (mM) and temperatures.

DMOT conc.	313 K	323 K	333 K
Blank	1.44	1.71	3.02
0.10	0.96	1.18	2.13
0.40	0.47	0.86	1.58
1.00	0.41	0.59	1.45
2.00	0.28	0.51	1.04
4.00	0.19	0.37	0.73

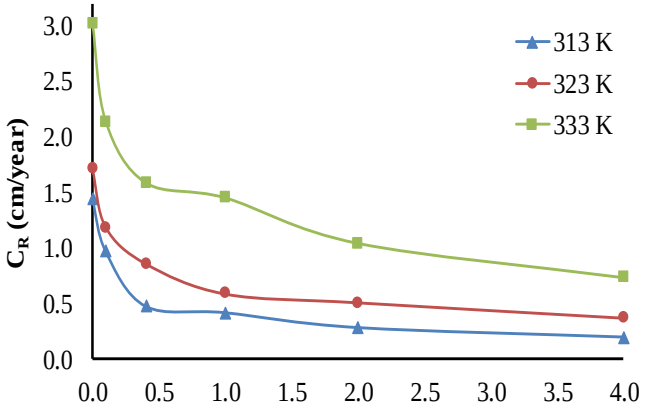

Fig. 3. Relation between corrosion rate and DMOT concentration at 313, 323, and 333 K.

C. Adsorption Isotherms

Since the corrosion process primarily takes place on the metal surface, studying thermodynamics and kinetics of the adsorption process at the metal-solution interface may reveal significant information about the adsorption behavior of inhibitor molecules on the metal surface. Adsorption isotherms are considered to be useful tools for studying the interaction/adsorption of inhibitors with/on metal surfaces [12,23]. Several adsorption isotherms have been developed and utilized in corrosion inhibition studies, e.g. Freundlich, Langmuir, Temkin, and Frumkin [6,7,19,27-29]. In the current study, the Langmuir adsorption isotherm has been used as it gives the best fit to our experimental results. In the Langmuir isotherm, the relation between the degree of surface coverage (θ) and the inhibitor concentration (C_{inh}) is governed by [7,19]:

$$\frac{C_{inh}}{\theta} = \frac{1}{K_{ads}} + C_{inh} \qquad (6)$$

where K_{ads} is the equilibrium constant for the inhibitor adsorption-desorption processes. The degree of surface coverage (θ) values (see Table 2) were calculated from potentiodynamic polarization measurements using Eq. 2.

Table 4: Thermodynamic parameters for the adsorption of DMOT on the mild steel surface at different temperatures (K).*

T	K_{ads}	ΔG_{ads}	ΔH_{ads}	ΔS_{ads}
313	4632.2	-32.4	-28.6	12.4
323	3410.5	-32.6		
333	2394.3	-32.7		

* ΔG_{ads} and ΔH_{ads} in (kJ mol^{-1}), ΔS_{ads} in (J mol^{-1} K^{-1}).

Linear plots ($R^2 \approx 1$) of $\frac{C_{inh}}{\theta}$ versus C_{inh} at the three studied temperatures are shown in Figure 4. The values of K_{ads} at the three temperatures were obtained from the intercepts of the plots (see Table 4).

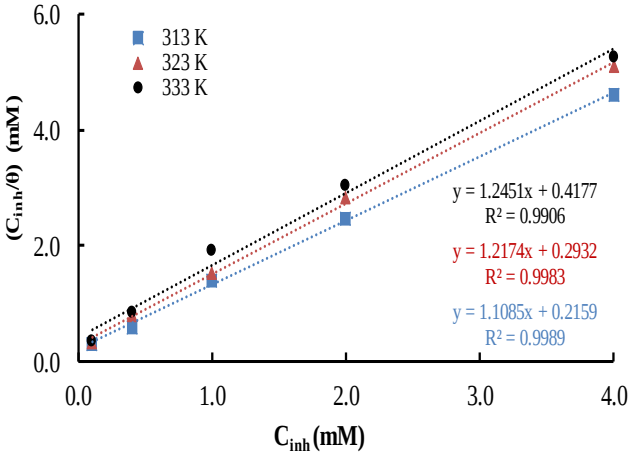

Fig. 4. Langmuir adsorption isotherm of DMOT on the surface of mild steel at 313, 323, and 333 K.

From K_{ads} values, the standard free energies (ΔG_{ads}), enthalpies (ΔH_{ads}), entropies (ΔS_{ads}) of adsorption at the three temperatures were calculated using the following two equations [1,6,23]:

$$\Delta G_{ads} = -RT \ln(55.5 K_{ads}) \qquad (7)$$

$$\ln K_{ads} = -\frac{\Delta H_{ads}}{RT} + \frac{\Delta S_{ads}}{R} + \ln\left(\frac{1}{55.5}\right) \qquad (8)$$

where R is the universal gas constant, T is the absolute temperature, and 55.5 is the molar concentration of H_2O in mol L^{-1}. In order to obtain ΔH_{ads} and ΔS_{ads} from Eq. 8, $\ln K_{ads}$ should be plotted against $1/T$, such a plot is depicted in Figure 5.

The calculated thermodynamic parameters (K_{ads}, ΔG_{ads}, ΔH_{ads}, and ΔS_{ads}) are summarized in Table 4.

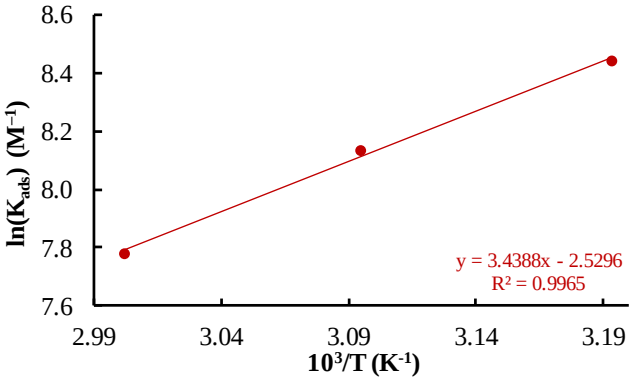

Fig. 5. Ln (K_{ads}) versus reciprocal of temperature for adsorption of DMOT on the mild steel surface.

The negative signs of both ΔG_{ads} and ΔH_{ads} and the positive sign of ΔS_{ads} indicate that the adsorption of DMOT on mild steel surface is a spontaneous process at all studied temperatures [2,3,19]. In general, the physical adsorption (physisorption) is related to values of $-\Delta G_{ads} < 20$ while the chemical adsorption (chemisorption) is related to values of $-\Delta G_{ads} > 40$ [8,19,23,31]. In this investigation, the obtained values of ΔG_{ads} are (~ –32 kJ mol^{-1}) at the three studied temperatures, thus suggesting that the adsorption of DMOT molecules on the mild steel surface is a mixed-type adsorption, i.e., involves both physisorption and chemisorption. This adsorption is also an exothermic process, $\Delta H_{ads} = -28.6$ kJ mol^{-1}, associated with an increase of entropy, $\Delta S_{ads} = 12.4$ J mol^{-1} K^{-1} (Table 4). The positive sign of ΔS_{ads} indicates that the adsorption of DMOT occurs on the mild steel surface can be considered as a quasi-substitution process between the molecules of DMOT and the molecules of water [8]. Therefore, the increase of entropy is due to the increase of the system's disorder as the number of water molecules being desorbed is greater than the number of DMOT molecules being adsorbed.

D. Kinetic Parameters

In order to give more insight into the adsorption of DMOT inhibitor on the mild steel surface in HCl solutions, some activation parameters are determined in this study. The activation energies (E_a), enthalpies ($\Delta H^{\ddagger}$), and entropies ($\Delta S^{\ddagger}$) were calculated using the Arrhenius and transition state equations [1,23,29]:

$$\ln(i_{corr}) = \ln(A) - \frac{E_a}{RT} \quad (9)$$

$$\ln\left(\frac{i_{corr}}{T}\right) = -\frac{\Delta H^{\ddagger}}{RT} + \frac{\Delta S^{\ddagger}}{R} + \ln\left(\frac{R}{Nh}\right) \quad (10)$$

where i_{corr} is the corrosion current density, A is the Arrhenius pre-exponential constant, R is the universal gas constant, T is the absolute temperature, N is Avogadro's number, and h is Planck's constant. According to Eqs. 9 and 10, the plots of $\ln(i_{corr})$ versus $1/T$ (as shown in Figure 6) and $\ln\left(\frac{i_{corr}}{T}\right)$ versus $1/T$ (as shown in Figure 7) give straight lines. From the slopes and intercepts of the straight lines, E_a, $\Delta H^{\ddagger}$, and $\Delta S^{\ddagger}$ were obtained and are listed in Table 5.

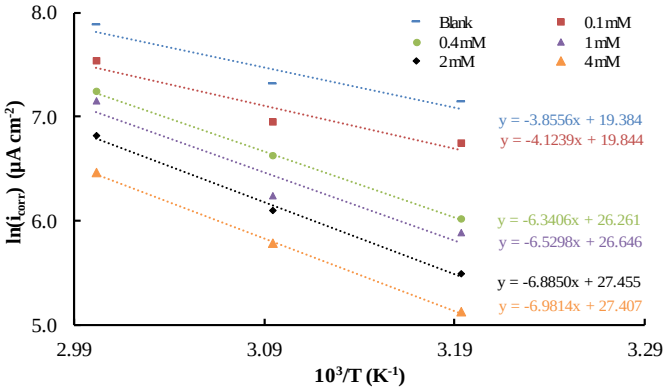

Fig. 6. Arrhenius plots of ln(i_{corr}) versus reciprocal of temperature for mild steel corrosion in the absence and presence of 0.1, 0.4, 1, 2, and 4 mM of DMOT.

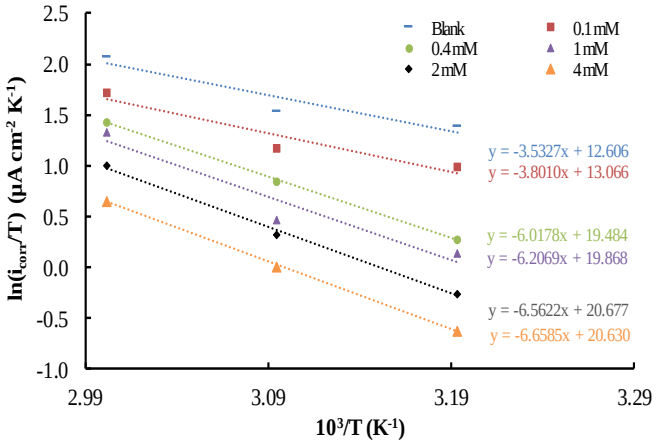

Fig. 7. Transition state plots of ln(i_{corr}/T) versus reciprocal of temperature for mild steel corrosion in the absence and presence of 0.1, 0.4, 1, 2, and 4 mM of DMOT.

Table 5: Kinetic parameters for the adsorption of DMOT on mild steel surface with different DMOT concentrations. *

DMOT Conc.	E_a	$\Delta H^{\ddagger}$	$\Delta S^{\ddagger}$
Blank	32.1	29.4	-92.7
0.10	34.3	31.6	-88.9
0.40	52.7	50.0	-35.6
1.00	54.3	51.6	-32.4
2.00	57.2	54.6	-25.6
4.00	58.0	55.4	-26.0

* E_a and $\Delta H^{\ddagger}$ in (kJ mol^{-1}), and $\Delta S^{\ddagger}$ in (J mol^{-1} K^{-1}).

Values of E_a and $\Delta H^{\ddagger}$ are lower without DMOT than with it. Moreover, both E_a and $\Delta H^{\ddagger}$ increase as the concentration of DMOT increases. These results clearly reveal that the corrosion of mild steel is inhibited by the presence of DMOT and the inhibition effect is enhanced with increasing DMOT concentration. The entropy of activation ($\Delta S^{\ddagger}$) goes to more positive values as the DMOT concentration increases that indicates a dissociative mechanism (dissolution) in which the system's disorder increases when going from reactants to the activated complex in the rate-determining step [8].

E. Characteristics of Corrosion Products on Mild Steel Surface

- **Scanning Electron Microscopy**

Scanning electron microscopy (SEM) was performed after corrosion tests were completed to investigate the morphology of the mild steel specimen surfaces. SEM micrographs for mild steel specimens after immersion in a HCl solution in the absence (a) and in presence (b) of 4.0 mM DMOT at 313, 323, and 333 K are shown in Figures 8, 9, and 10 respectively.

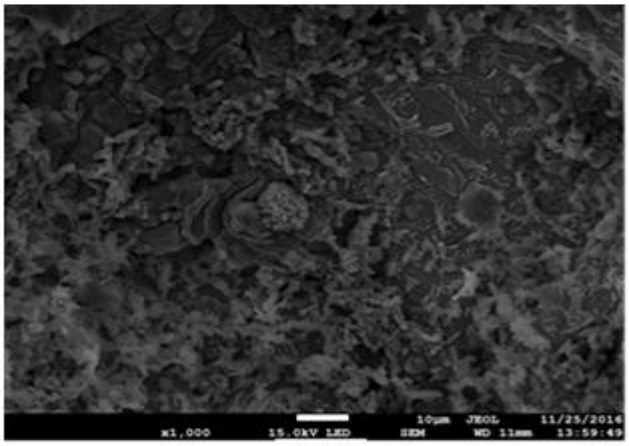

(a)

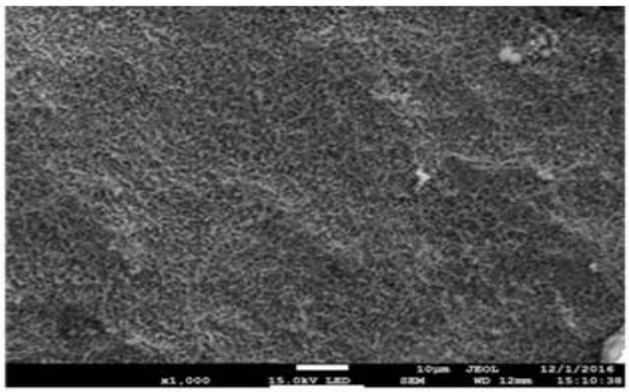

(b)

Fig. 8. SEM micrographs for the surface of mild steel specimens after immersion in HCl solution at 313 K; (a) in absence and (b) in presence of 4mM DMOT.

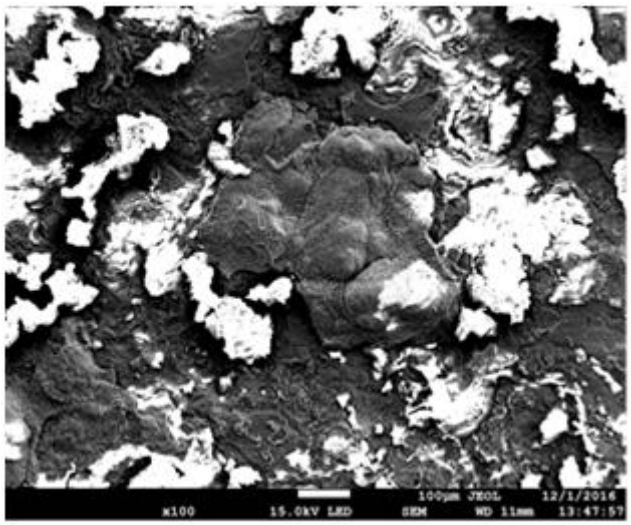

(a)

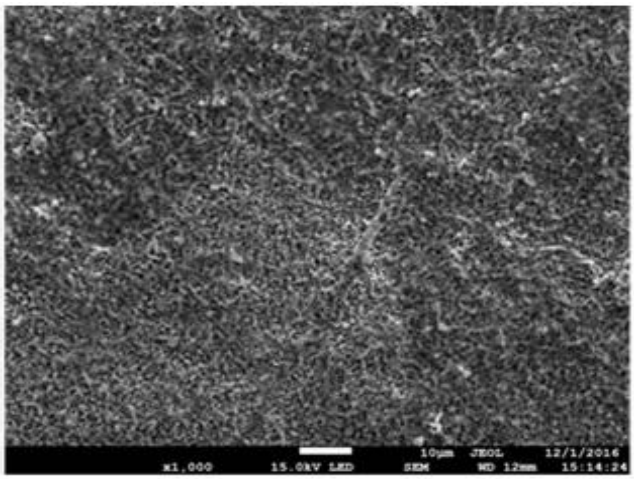

(b)

Fig. 9. SEM micrographs for the surface of mild steel specimens after immersion in HCl solution at 323 K; (a) in absence and (b) in presence of 4mM DMOT.

SEM micrographs reveal non uniform, highly corroded surfaces in the absence of DMOT inhibitor due to the dissolution of the surfaces in the aggressive acid solution (see Figures 8a, 9a, and 10a). By contrast, the presence of 4mM DMOT inhibitor represses corrosion resulting in uniformly less corroded surfaces when compared with surfaces without inhibitor (see Figures 8b, 9b, and 10b). It can be seen from Figures 8, 9, and 10 that surface damage increases with increasing temperature. This is due to the fact that adsorption of DMOT molecules declines as the temperature increases, and with declining adsorption the area of the mild steel surface exposed to acid attack increases and, consequently, there is greater corrosion and surface damage.

- **Energy Dispersive Spectroscopy**

Fig. 10. SEM micrographs for the surface of mild steel specimens after immersion in HCl solution at 333 K; (a) in absence and (b) in presence of 4mM DMOT.

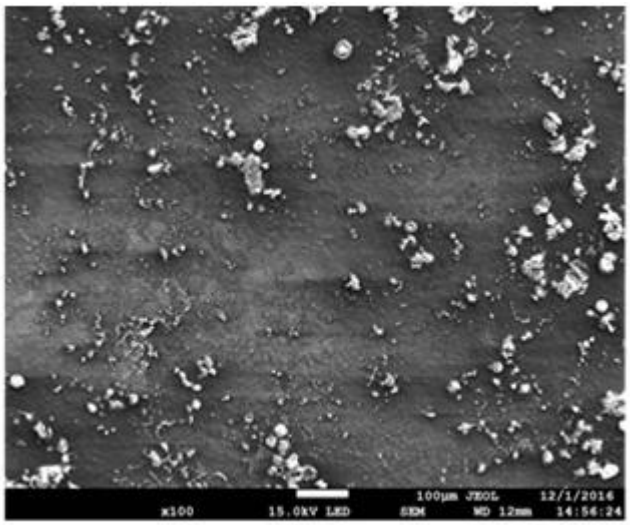

(b)

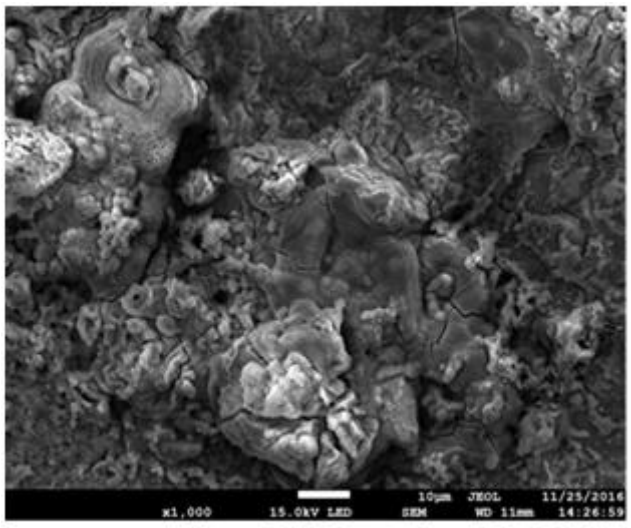

(a)

Fig. 10. SEM micrographs for the surface of mild steel specimens after immersion in HCl solution at 333 K; (a) in absence and (b) in presence of 4mM DMOT.

The energy dispersive spectroscopy (EDS) technique has been used to evaluate the chemical elements present as a result of corrosion on the metal surfaces [23] In this study, EDS was utilized to determine major elements: iron, oxygen, carbon, silicon, manganese and chlorine in the corroded mild steel surfaces as shown in Figure 11. In the absence of DMOT, the EDS spectrum (Figure 11a) presents the characteristic peaks of chemical elements in the surface corroded in the absence of DMOT. In the presence of DMOT, the EDS spectrum (Figure 11b) shows additional peaks for nitrogen and sulfur elements. These additional peaks (especially the N peak) indicate the adsorption of DMOT molecules. As can be seen in Figure 11, the EDS spectrum in the presence of DMOT shows more intense iron peaks than the EDS spectrum when DMOT is absent which indicates that there is less dissolution of iron when the mild steel surface is protected by an adsorption layer of DMOT.

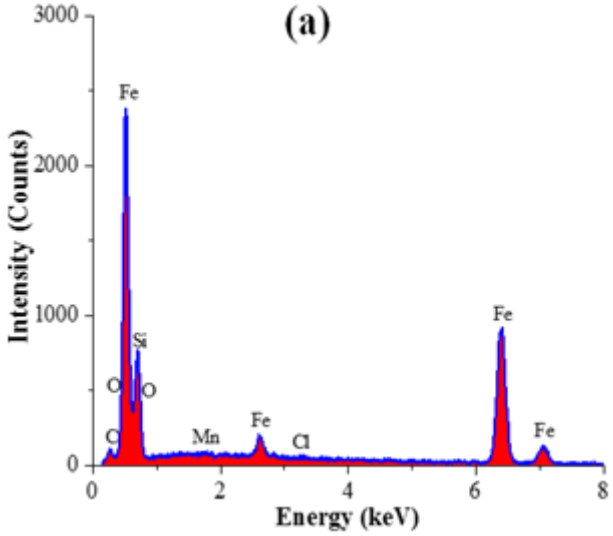

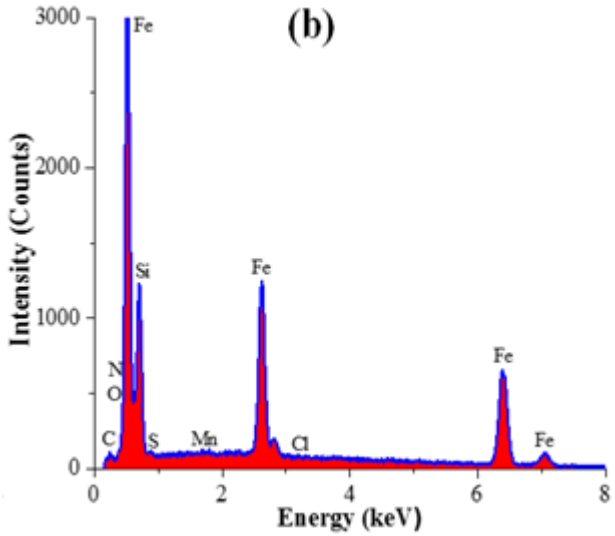

Fig. 11. EDS spectra for the surface of mild steel specimens after immersion in HCl solution at 313 K; (a) in absence and (b) in presence of 4mM DMOT.

- **X-Ray Diffraction Analysis**

X-ray diffraction (XRD) analysis gives qualitative and quantitative information about corrosion products formed on metal surfaces [2,23]. The XRD patterns of the mild steel corrosion products at 313 K in the absence and presence of 4.0 mM DMOT are shown in Figures 12a and 12b, respectively.

In the absence of DMOT, the XRD peaks detected various phases including Fe_2O_3 (hematite) at $2\theta = 16^o$, Fe_4O_3Cl (akageneite) at $2\theta = 21^o$, Fe_3O_4 (magnetite) at $2\theta = 27^o$, 36^o, 56^o, FeOOH (goethite) at $2\theta = 38^o$, $FeCO_3$ (Siderite) at $2\theta = 63^o$, and Fe (matrix) at $2\theta = 45^o$, 83^o. In the presence of DMOT, the XRD peaks are identified with dominant Fe_3O_4 (magnetite) at $2\theta = 27^o$, 36^o, and Fe (matrix) at $2\theta = 45^o$, 65^o, 83^o only. It is obvious from the XRD analysis that mild steel surface in the absence of DMOT inhibitor contains more corrosion products and less iron peaks than the surface protected by inhibitor. These XRD results indicate adsorption of DMOT molecules which results in a reduction of corrosion.

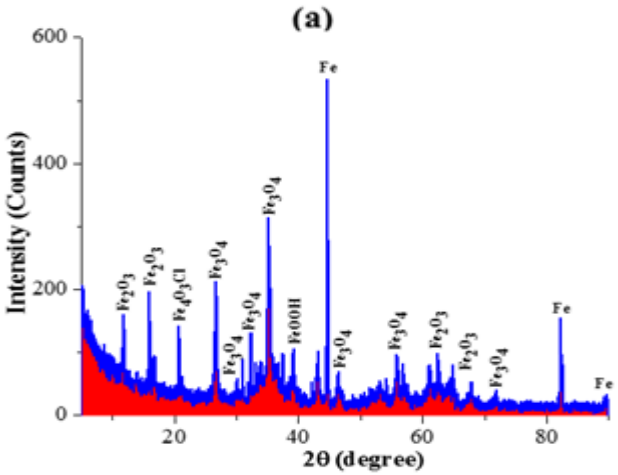

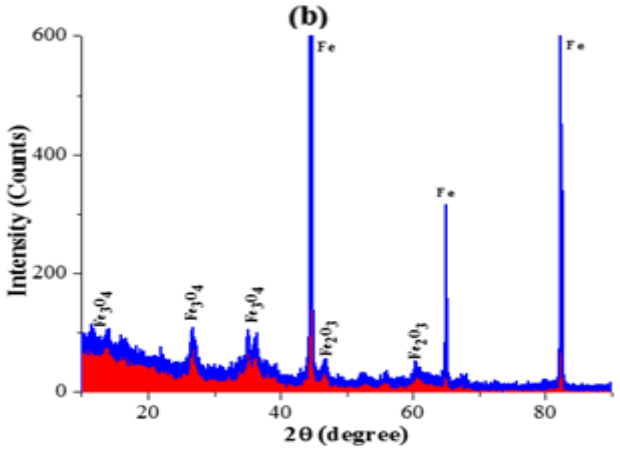

Fig. 12. X-ray diffraction pattern of phases present on the surface of mild steel specimens after immersion in HCl solution 313 K; (a) in absence and (b) in presence of 4mM DMOT.

F. Quantum Chemical Considerations

Quantum chemical methods have become valuable tools in the study of atoms and molecules and in modeling complex systems in chemistry, biology, pharmacology, materials science and engineering, and many other areas [2,12,14,25,29]. One of quantum chemical methods successfully used in the study of corrosion inhibition is density functional theory (DFT) [4,13,19,28]. DFT calculations were performed in this work to correlate the molecular structure and properties of DMOT and $DMOTH^+$ with their inhibition action to gain a better understanding of their inhibitory effect.

In acidic solution, DMOT can exist in neutral and/or protonated species. Since DMOT has three heteroatoms (N, O, and S), it can be protonated at any of these atoms as shown in Figure 13. Proton affinities and basicities (in kJ mol^{-1}) for the three reactions in Figure 13 were calculated and listed in Table 6 as well as the total electronic energies (in hartree) for the three possible protonated forms of DMOT. Proton affinities and basicities are calculated (using B3LYP in the gas phase) as the negative of enthalpies and Gibbs energies, respectively, of the three reactions in Figure 13. It can be seen from Table 6 that DMOT protonated at the S atom has highest proton affinity and basicity values and the lowest total energy value (more stable) among the three protonated forms. Thus, the most favorable $DMOTH^+$ form results as the protonation occurs only at the S atom.

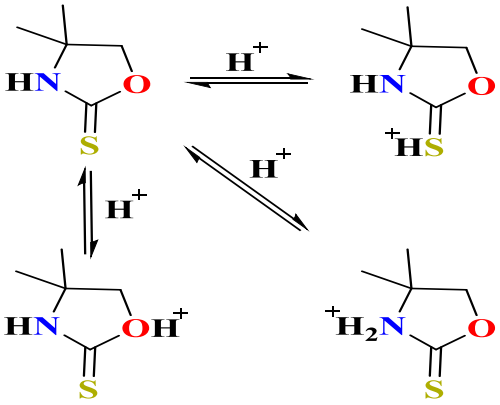

Fig. 13. Different possible sites for the protonation of DMOT.

Table 6: Proton Affinities and Basicities of DMOT (in kJ mol^{-1}) at 298.15 K and total energies (in hartree) for its possible protonated forms obtained using B3LYP/6-31G(d) in the gas phase.

Protonation Site	Proton Affinity	Basicity	Total Energy
N	790	800	-724.5423
O	747	766	-724.5143
S	871	885	-724.5583

The optimized structures of DMOT and $DMOTH^+$ as obtained using B3LYP/6-31G(d) with PCM in aqueous solution are shown in Figure 14. Density distributions of the frontier molecular orbitals (HOMO and LUMO) of DMOT and $DMOTH^+$ are shown in Figure 15 and 16, respectively. Energies of the HOMO and LUMO (E_{HOMO} and E_{LUMO}) and their gap (ΔE_{HL}), the ionization potential (I), electron affinity (A), dipole moment (μ), absolute electronegativity (χ), absolute hardness (η), softness (σ), and number of electrons transferred (ΔN), of both DMOT and $DMOTH^+$ are presented in Table 7.

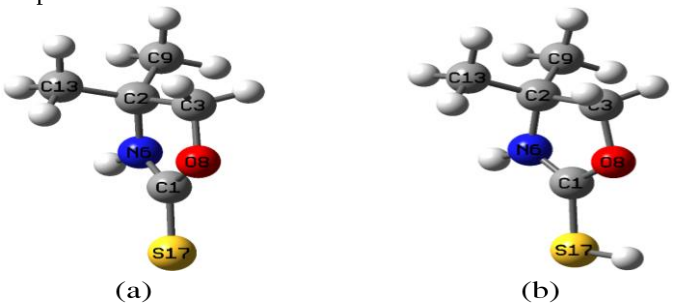

Fig. 14. Optimized geometries of (a) DMOT and (b) $DMOTH^+$ obtained using B3LYP/6-31G(d) with PCM in aqueous solution.

According to the theory of frontier molecular orbitals, interactions between inhibitor molecules and metal atoms take place via donations of electron densities from the highest occupied molecular orbital of the inhibitor (HOMO) to d-orbitals of the metal atoms, and/or via transferring of electron densities from d-orbitals of metal atoms to the lowest unoccupied molecular orbital (LUMO) of the inhibitor [2,12,13,19,25]. Thus, the tendency of an inhibitor to donate or accept electrons can be measured by E_{HOMO} and E_{LUMO}, respectively. A high value of $-E_{HOMO}$ (i.e., ionization potential) refers to a low ability of the inhibitor to donate electrons, and vice versa. A high value of $-E_{LUMO}$ (i.e., electron affinity) refers to a high ability of the inhibitor to accept electrons, and vice versa. The energy gap between HOMO and LUMO orbitals (ΔE_{HL}) measures the ability of a molecule to transfer electrons between its HOMO and LUMO orbitals [2,4,19,28]. Therefore, the lower ΔE_{HL} an inhibitor has, the higher its inhibition efficiency. The electron density of the HOMO of DMOT localizes mainly at the sulfur atom, whereas the density of the LUMO spreads out on sulfur, oxygen, nitrogen, and carbon (C1) atoms as shown in Figure 15. This means that the oxygen, nitrogen, and carbon (C1) atoms are the active sites of DMOT responsible for receiving electrons from d-orbitals of the mild steel atoms,

while the sulfur atom represents the active site of DMOT responsible for both donating and accepting electrons to/from the mild steel atoms. After protonation, major changes of HOMO and LUMO distributions are observed as shown in Figure 16. The HOMO density is spreads out on sulfur, oxygen, nitrogen, and carbon (C1) atoms indicating the tendency of these sites to donate electrons, while the LUMO density is located mainly at the sulfur and carbon (C1) atoms indicating the tendency of these sites to accept electrons.

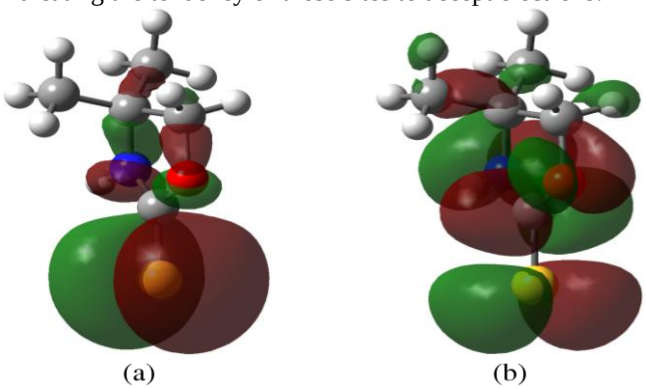

Fig. 15. Electron density distributions for frontier molecule orbitals of DMOT obtained at B3LYP/6-31G(d) with PCM in aqueous solution; (a) HOMO and (b) LUMO.

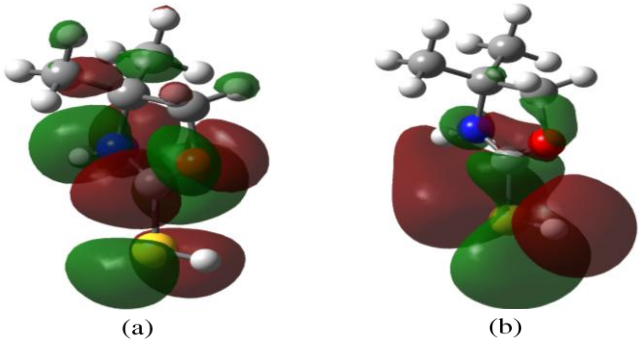

Fig. 16. Electron density distributions for frontier molecule orbitals of DMOTH$^+$ obtained at B3LYP/6-31G(d) with PCM in aqueous solution; (a) HOMO and (b) LUMO.

It can be seen from Table 7 that the E_{HOMO} of DMOT is -6.26 eV (i.e. I = 6.26 eV) which is considered to be a somewhat high ionization energy indicating that DMOT has a low ability to donate electrons to the mild steel atoms. After protonation, a remarkable decrease in E_{HOMO} (increase in I) is observed indicating that DMOTH$^+$ has a lower tendency to donate electrons than DMOT. On the other hand, E_{LUMO} and A values indicate that both DMOT and DMOTH$^+$ have high abilities (DMOTH$^+$ > DMOT) to accept electrons from mild steel atoms. Dipole moments (μ) and the number of electrons transferred (ΔN) are other important electronic parameters in predicting inhibition efficiencies and inhibition mechanisms of inhibitors [4]. The high value of the DMOT dipole moment ($\mu = 9.42$ Debye) implies strong dipole-dipole interactions between DMOT and the mild steel atoms and, therefore, a strong ability to be directly adsorbed on the mild steel surface and replace H_2O molecules. On the other hand, DMOTH$^+$ has a very low dipole moment ($\mu = 0.60$ Debye), hence it has a low ability to be directly adsorbed on the mild steel surface. However, DMOTH$^+$ molecules can be electrostatically interacting with Cl^- on the mild steel surface and replace H^+ ions. The negative sign of ΔN for both DMOT and DMOTH$^+$ reveals that they have the ability to receive electrons, that is, electrons transfer from the mild steel atoms to DMOT and DMOTH$^+$.

Table 7: Quantum chemical parameters (in eV and μ in Debye) of DMOT and DMOTH$^+$ calculated using B3LYP/6-31G(d) with PCM in aqueous solution.

Parameter	Table 7: Quantum chemical parameters (in eV and μ in Debye) of DMOT and DMOTH$^+$ calculated using B3LYP/6-31G(d) with PCM in aqueous solution. DMOT	DMOTH$^+$
E_{HOMO}	-6.26	-8.34
E_{LUMO}	-0.44	-1.58
ΔE_{AH}	5.82	6.76
I	6.26	8.34
A	0.44	1.58
μ	9.42	0.6
ΔN	-0.63	-0.3
χ	3.35	4.96
η	2.91	3.38
σ	0.34	0.3

The electronegativity of DMOTH$^+$ (4.96 eV) is higher than that of DMOT (3.35 eV) indicating the higher capability of DMOTH$^+$ to accept electrons from d-orbitals of the metal atoms than that of DMOT. In contrast,
Table 7 shows that the ΔE_{HL} and η are higher and σ is lower for DMOTH$^+$ comparing to those for DMOT.
In general, an inhibitor with higher values of ΔE_{HL} and η and lower value of σ displays weak interactions with the metal surface (i.e., has low inhibition efficiency) [28,38,39,40]. It can be concluded from the above discussion that the DMOT molecules have a stronger tendency to adsorb on the mild steel surface via dipole-dipole interaction and the DMOTH$^+$ molecules have a superior tendency to accept electrons from d-orbitals of the metal atoms.

Fukui functions for DMOT and DMOTH$^+$ obtained using B3LYP/6-31G(d) are shown in Table 8. The Fukui functions were calculated to explore the local reactivity sites of the inhibitor molecules. Generally, high values of f_k^+ and f_k^- are associated with preferred sites for nucleophilic attacks (by electron rich species) and electrophilic attacks (by electron-poor species), respectively. It is clear from Table 8 that sulfur, oxygen, nitrogen, and carbon (C1) atoms in both DMOT and DMOTH$^+$ are the most susceptible sites toward nucleophilic attacks as they have largest f_k^+ values. On the other hand, sulfur atom in DMOT and both sulfur and nitrogen atoms in DMOTH$^+$ are the most preferred sites for electrophilic attack as they have largest f_k^-. Based on the previous discussion, the adsorption mechanism of the DMOT and DMOTH$^+$ inhibitor can be described as follows:

(i) the DMOT or $DMOTH^+$ molecules adsorb strongly on the mild steel surface via dipole-dipole or electrostatic interactions (physisorption), (ii) the DMOT or $DMOTH^+$ molecules can also be chemically adsorbed (chemisorption) via forming back-bonds between the anti-bonding orbitals (most likely LUMOs) of DMOT molecules and d-orbitals of the mild steel atoms.

Table 8: Fukui functions for DMOT and $DMOTH^+$ obtained using B3LYP/6-31G(d) with PCM in aqueous solution.

No.	Atom	DMOT		$DMOTH^+$	
		f_k^+	f_k^-	f_k^+	f_k^-
1	C	**0.2049**	0.0624	**0.2179**	0.0476
2	C	0.0144	0.0106	0.0148	0.0245
3	C	0.0234	0.0175	0.0258	0.0188
4	H	0.0276	0.0141	0.0280	0.0209
5	H	0.0252	0.0160	0.0276	0.0204
6	N	**0.0966**	0.0487	**0.1197**	**0.1341**
7	H	0.0493	0.0277	0.0542	0.0423
8	O	**0.0897**	0.0432	**0.1071**	0.0462
9	C	0.0126	0.0089	0.0143	0.0274
10	H	0.0124	0.0076	0.0141	0.0170
11	H	0.0160	0.0104	0.0197	0.0237
12	H	0.0116	0.0067	0.0123	0.0179
13	C	0.0135	0.0066	0.0146	0.0304
14	H	0.0200	0.0096	0.0206	0.0254
15	H	0.0133	0.0070	0.0143	0.0179
16	H	0.0104	0.0056	0.0121	0.0182
17	S	**0.3589**	**0.6974**	**0.2385**	**0.4065**
18	H	-	-	0.0440	0.0606

IV. CONCLUSION

The inhibitory effect of DMOT and $DMOTH^+$ on corrosion of mild steel in 1 M HCl solution at 313, 323, and 333 K has been investigated using both electrochemical techniques and DFT calculations. The study shows that DMOT is an effective inhibitor for corrosion of mild steel in 1 M HCl solution at all studied temperatures, and that its inhibition efficiency increases with increasing DMOT concentration and decreases with increasing temperature. Also, the corrosion rate is found to decrease with increasing DMOT concentration and increase with increasing temperature. Results obtained from potentiodynamic polarization measurements are in good agreement with the adsorption, kinetic, and DFT results. The adsorption of DMOT on the mild steel surface is found to obey the Langmuir isotherm and to be a mixed-type process, i.e. involves both physisorption and chemisorption. Signs of ΔG_{ads}, ΔH_{ads}, and ΔS_{ads} indicate that the adsorption of DMOT on the mild steel surface is a spontaneous process at all studied temperatures. The positive sign of ΔS_{ads} indicates that the adsorption of DMOT on the mild steel surface can be considered as a quasi-substitution process between molecules of DMOT and molecules of water. The SEM micrographs show heavily corroded mild steel specimen surfaces in the HCl solution in the absence of DMOT, while they show smooth and less corroded surfaces in the presence of DMOT as result of the DMOT inhibition action. DFT calculations reveals that DMOT or $DMOTH^+$ molecules adsorb strongly on the mild steel surface via dipole-dipole or electrostatic interactions (physisorption), and they can also be chemically adsorbed (chemisorption) via forming back-bonds between the anti-bonding orbitals of DMOT or $DMOTH^+$ molecules and d-orbitals of the mild steel atoms.

The results obtained from quantum chemical calculations are in agreement with the results obtained from our experimental work.

ACKNOWLEDGMENT

The authors are thankful to the Western Canadian Research Grid (WestGrid), the Atlantic Computational Excellence Network (ACEnet), and Compute Canada for providing the computational facilities.

REFERENCES

1. A.Y. Musa, A.A.H. Kadhum, A.B. Mohamad, A.R. Daud, M.S. Takriff, S.K. Kamarudin, A comparative study of the corrosion inhibition of mild steel in sulphuric acid by 4,4-dimethyloxazolidine-2-thione, Corros. Sci. 51 (2009) 2393–2399. doi:10.1016/j.corsci.2009.06.024.
2. M. Muralisankar, R. Sreedharan, S. Sujith, N.S.P. Bhuvanesh, A. Sreekanth, N(1)-pentyl isatin-N(4)-methyl-N(4)-phenyl thiosemicarbazone (PITSc) as a corrosion inhibitor on mild steel in HCl, J. Alloys Compd. 695 (2017) 171–182. doi:10.1016/j.jallcom.2016.10.173.
3. A.M. Mobin, M. Rizvi, Adsorption and corrosion inhibition behavior of hydroxyethyl cellulose and synergistic surfactants additives for carbon steel in 1 M HCl, Carbohydr. Polym. 156 (2017) 202–214. doi:10.1016/j.carbpol.2016.08.066.
4. A. Dutta, S.K. Saha, P. Banerjee, A.K. Patra, D. Sukul, Evaluating corrosion inhibition property of some Schiff bases for mild steel in 1 M HCl: competitive effect of the heteroatom and stereochemical conformation of the molecule, RSC Adv. 6 (2016) 74833–74844. doi:10.1039/C6RA03521C.
5. Z. Tao, S. Zhang, W. Li, B. Hou, Corrosion inhibition of mild steel in acidic solution by some oxo-triazole derivatives, Corros. Sci. 51 (2009) 2588–2595. doi:10.1016/j.corsci.2009.06.042.
6. N. Soltani, Corrosion Inhibition of Low Carbon Steel by Strychnos nux- vomica Extract as Green Corrosion Inhibitor in Hydrochloric Acid Solution, Int. J. Electrochem. Sci. 11 (2016) 8827–8847. doi:10.20964/2016.10.22.
7. M.A. Deyab, Adsorption and inhibition effect of Ascorbyl palmitate on corrosion of carbon steel in ethanol blended gasoline containing water as a contaminant, Corros. Sci. 80 (2014) 359–365. doi:10.1016/j.corsci.2013.11.056.
8. A.Karimi, I. Danaee, H. Eskandari, M. RashvanAvei, Adsorption isotherm and inhibition effect of a synthesized di-(m-Formylphenol)-1,2-cyclohexandiimine on corrosion of steel X52 in HCl solution, J. Cent. South Univ. 23 (2016) 249–257. doi:10.1007/s11771-016-3068-2.
9. F. Bentiss, M. Traisnel, M. Lagrenee, The substituted 1, 3, 4-oxadiazoles : a new class of corrosion inhibitors of mild steel in acidic media, Corros. Sci. 42 (2000) 127–146. doi:10.1016/S0010-938X(99)00049-9.
10. A. Mohamed, J.R. Cahoon, W.F. Caley, Anodic polarization behaviour of nickel-based alloys in neutral and very acidic solutions, 15 (2012) 1–30.
11. A.Y. Musa, A.A. Khadom, A.A.H. Kadhum, A.B. Mohamad, M.S. Takriff, Kinetic behavior of mild steel corrosion inhibition by 4-amino-5-phenyl-4H-1,2,4-trizole-3-thiol, J. Taiwan Inst. Chem. Eng. 41 (2010) 126–128. doi:10.1016/j.jtice.2009.08.002.
12. R. Yildiz, An electrochemical and theoretical evaluation of 4,6-diamino-2-pyrimidinethiol as a corrosion inhibitor for mild steel in HCl solutions, Corros. Sci. 90 (2015) 544–553. doi:10.1016/j.corsci.2014.10.047.
13. X. Zheng, S. Zhang, W. Li, L. Yin, J. He, J. Wu, Investigation of 1-butyl-3-methyl-1H-benzimidazolium iodide as inhibitor for mild steel in sulfuric acid solution, Corros. Sci. 80 (2014) 383–392. doi:10.1016/j.corsci.2013.11.053.

14. M. Yadav, R.R. Sinha, S. Kumar, T.K. Sarkar, Corrosion inhibition effect of spiropyrimidinethiones on mild steel in 15% HCl solution: Insight from electrochemical and quantum studies, RSC Adv. 5 (2015) 70832–70848. doi:10.1039/c5ra14406j.
15. R. Solmaz, Investigation of adsorption and corrosion inhibition of mild steel in hydrochloric acid solution by 5-(4-Dimethylaminobenzylidene)rhodanine, Corros. Sci. 79 (2014) 169–176. doi:10.1016/j.corsci.2013.11.001.
16. E.-S.M. Sherif, Corrosion inhibition in 2.0M sulfuric acid solutions of high strength maraging steel by aminophenyl tetrazole as a corrosion inhibitor, Appl. Surf. Sci. 292 (2014) 190–196. doi:10.1016/j.apsusc.2013.11.110.
17. S. Paramasivam, K. Kulanthai, G. Sadhasivam, R. Subramani, Corrosion inhibition of mild steel in hydrochloric acid using 4-(pyridin-2yl)-N-p-tolylpiperazine-1-carboxamide, Int. J. Electrochem. Sci. 11 (2016) 3393–3414. doi:10.20964/10109.
18. A.Y. Musa, A.A.H. Kadhum, A.B. Mohamad, M.S. Takriff, A.R. Daud, S.K. Kamarudin, On the inhibition of mild steel corrosion by 4-amino-5-phenyl-4H-1, 2, 4-trizole-3-thiol, Corros. Sci. 52 (2010) 526–533. doi:10.1016/j.corsci.2009.10.009.
19. L. Guo, S.T. Zhang, W.P. Li, G. Hu, X. Li, Experimental and computational studies of two antibacterial drugs as corrosion inhibitors for mild steel in acid media, Mater. Corros. (2013) n/a-n/a. doi:10.1002/maco.201307346.
20. R. Yıldız, A. Döner, T. Doğan, İ. Dehri, Experimental studies of 2-pyridinecarbonitrile as corrosion inhibitor for mild steel in hydrochloric acid solution, Corros. Sci. 82 (2014) 125–132. doi:10.1016/j.corsci.2014.01.008.
21. M. Bouanis, M. Tourabi, A. Nyassi, A. Zarrouk, C. Jama, F. Bentiss, Corrosion inhibition performance of 2,5-bis(4-dimethylaminophenyl)-1,3,4-oxadiazole for carbon steel in HCl solution: Gravimetric, electrochemical and XPS studies, Applied Surface Science 389 (2016) 952–966. doi:10.1016/j.apsusc.2016.07.115
22. A.Y. El-Etre, A.I. Ali, A Novel Green Inhibitor for C- Steel Corrosion in 2.0Mol·L−1 Hydrochloric Acid Solution, Chinese J. Chem. Eng. (2016) 1–8. doi:10.1016/j.cjche.2016.08.017.
23. D.K. Verma, F. Khan, Corrosion inhibition of mild steel in hydrochloric acid using extract of glycine max leaves, Res Chem Intermed. 42 (2016) 3489–3506. DOI 10.1007/s11164-015-2227-7.
24. A.M. Al-Fakih, M. Aziz, H.M. Sirat, Turmeric and ginger as green inhibitors of mild steel corrosion in acidic medium, J. Mater. Environ. Sci. 6 (2015) 1480–1487.
25. S. Benabid, T. Douadi, S. Issaadi, C. Penverne, S. Chafaa, Electrochemical and DFT studies of a new synthesized Schiff base as corrosion inhibitor in 1M HCl, Measurement. 99 (2016) 53–63. doi:10.1016/j.measurement.2016.12.022.
26. A.A. Al-Amiery, A.A.H. Kadhum, A.H.M. Alobaidy, A.B. Mohamad, P.S. Hoon, Novel corrosion inhibitor for mild steel in HCL, Materials (Basel). 7 (2014) 662–672. doi:10.3390/ma7020662.
27. S. Manimegalai, P. Manjula, Thermodynamic and adsorption studies for corrosion inhibition of mild steel in aqueous media by Sargasam swartzii (Brown algae), J. Mater. Environ. Sci. 6 (2015) 1629–1637.
28. H.M. Abd El-Lateef, Experimental and computational investigation on the corrosion inhibition characteristics of mild steel by some novel synthesized imines in hydrochloric acid solutions, Corros. Sci. 92 (2015) 104–117. doi:10.1016/j.corsci.2014.11.040.
29. A.U. Ezeoke, O.G. Adeyemi, O.A. Akerele, N.O. Obi-egbedi, Computational and Experimental Studies of 4-Aminoantipyrine as Corrosion Inhibitor for Mild Steel in Sulphuric Acid Solution, 7 (2012) 534–553.
30. L. Elkadi, B. Mernari, M. Traisnel, F. Bentiss, M. Lagrenée, The inhibition action of 3,6-bis (2-methoxyphenyl)-1,2-dihydro-1,2,4,5-tetrazine on the corrosion of mild steel in acidic media, Corros. Sci. 42 (2000) 703–719.
31. A.Y. Musa, A.A.H. Kadhum, A.B. Mohamad, A.A.B. Rahoma, H. Mesmari, Electrochemical and quantum chemical calculations on 4,4-dimethyloxazolidine-2-thione as inhibitor for mild steel corrosion in hydrochloric acid, J. Mol. Struct. 969 (2010) 233–237. doi:10.1016/j.molstruc.2010.02.051.
32. ASTM G1-3 Standard Practice for Preparing, Cleaning, and Evaluating Corrosion Test Specimens. ASTM International: West Conshohocken, PA, USA, (2003).
33. M.J. Frisch, G.W. Trucks, H.B. Schlegel, G.E. Scuseria, M.A. Robb, J.R. Cheeseman, G. Scalmani, V. Barone, B. Mennucci, G.A. Petersson, et al. Gaussian 09, Revision D.01, (2009).
34. A.D. Becke, Density-Functional Thermochemistry. III. The Role of Exact Exchange. J. Chem. Phys. 98 (1993) 5648–5652.
35. C. Lee, W. Yang, R.G. Parr, Development of the Colle-Salvetti Correlation-Energy Formula into a Functional of the Electron Density. Phys. Rev. B 37 (1988) 785-789.
36. A.V. Marenich, C.J. Cramer, D.G. Truhlar, Universal Solvation Model Based on Solute Electron Density and on a Continuum Model of the Solvent Defined by the Bulk Dielectric Constant and Atomic Surface Tensions, J. Phys. Chem. B. 113 (2009) 6378–6396.
37. H. Ju, Z. Kai, Y. Li, Corros. Sci. 50 (2008) 865-871.
38. S.K. Saha, P. Banerjee, A theoretical approach to understand the inhibition mechanism of steel corrosion with two aminobenzonitrile inhibitors, RSC Adv. 5 (2015) 71120-71130.
39. N.K. Gupta, C. Verma, R. Salghi, H. Lgaz, A.K. Mukherjee, M.A. Quraishi, New phosphonate-based corrosion inhibitors for mild steel in hydrochloric acid useful for industrial pickling processes: experimental and theoretical approach, 41 (2017) 13114-13129.
40. A., Mohamed, A., Alrawashdeh, J. Pumwa, The Inhibition Performance of Thiadiazole Derivatives on The Steel Corrosion: DFT And QSAR Assessment, The Journal of Corrosion Science and Engineering, 22, 8 (2019) 1-23.

AUTHORS PROFILE

Aezeden Mohamed has a B.Sc., M.Sc., and PhD degrees in Mechanical and Manufacturing at the University of Manitoba, Canada. His areas of research are experimental in nature includes but not limited; mechanical properties, materials characterizations, corrosion and corrosion control, and biomedical engineering. He has carried out research and taught at the University of Manitoba and Memorial University in Canada. In addition to his technical research interests, he earned diploma in Higher Education Teaching from University of Manitoba, Canada. He has published over 10 papers in Canadian Engineering Education Association. Currently, he is a Senior Lecturer at the University of Technology, Papua New Guinea

Ahmad Rawashdeh PhD in Computational and quantum Chemistry, Memorial University of Newfoundland, 2015 Research interest: Theoretical Chemistry; Developing and formulating methods in electronic structure theory; Atoms in molecules by radial density; Development of quantum chemistry codes. Computational Chemistry; Study of reaction mechanisms for the deamination of adenine and its derivatives; Study of thermo-chemical properties of some molecules that found in the atmosphere or in human body.

Abdalhamid Rahoma PhD student in Process Engineering in Memorial University of Newfoundland and Labrador, St. John's, Canada.